Supporting Information

Free Energy Landscape and Dynamics of Supercoiled DNA by High-Speed Atomic Force Microscopy

Tine Brouns,[a] Herlinde De Keersmaecker,[a] Sebastian F. Konrad,[b] Noriyuki Kodera,[c] Toshio Ando,[c] Jan Lipfert,[b,*] Steven De Feyter,[a,*] and Willem Vanderlinden[a,b,*]

[a] *KU Leuven, Division of Molecular Imaging and Photonics, Celestijnenlaan 200F, 3001 Leuven, Belgium.*

[b] *Department of Physics, Nanosystems Initiative Munich, and Center for NanoScience, LMU Munich, Amalienstrasse 54, 80799 Munich, Germany.*

[c] *Nano-Life Science Institute (WPI-NanoLSI), Kanazawa University, Kakuma-machi, Kanazawa, 920-1192, Japan.*

Supplementary Movie: Supplementary Movie 1

File: Supplementary_Movie_1.avi

Title: Dynamics of positively supercoiled pBR322 on mica

Description: High-speed AFM image sequence of positively supercoiled pBR322 at the interface of muscovite mica and an aqueous buffer supplemented with 5 mM $MgCl_2$.

Movie parameters: Image size: 500 nm. Image acquisition speed: 0.6 s. (10 × real-time)

	2D	3D	3D-2D PROJECTED
PLL-MICA	A = 11 nm	A = 22 nm	A = 40 nm
	χ_{Red}^2 = 0.77	χ_{Red}^2 = 2.17	χ_{Red}^2 = 1.24
BARE MICA	A = 48 nm	A = 105 nm	A = 135 nm
	χ_{Red}^2 = 0.84	χ_{Red}^2 = 3.6	χ_{Red}^2 = 1.06

Supporting Table S1. Best fit parameters for end-end distance distributions of linear pBR322 adsorbed onto PLL-mica and bare mica, for different adsorption models: 2D equilibration ("2D"), kinetic trapping with conservation of the 3D end-end distance ("3D"), or kinetic trapping according to a 2D projection of the 3D end-end distance ("3D-2D projected"). For each adsorption model, 10^5 chains were simulated for a range of bending persistence lengths A and compared to the experimental distributions. The fitted persistence lengths A that yielded the lowest reduced chi-square value χ_{Red}^2 are listed for each model and for both deposition surfaces.

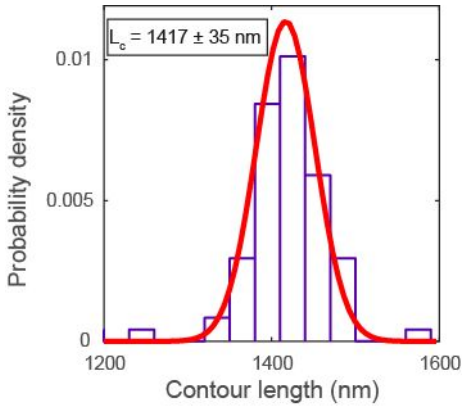

Supporting Figure S1. Contour length distribution as determined by automated tracing of linear pBR322 molecules adsorbed onto bare mica, and single Gaussian fit.

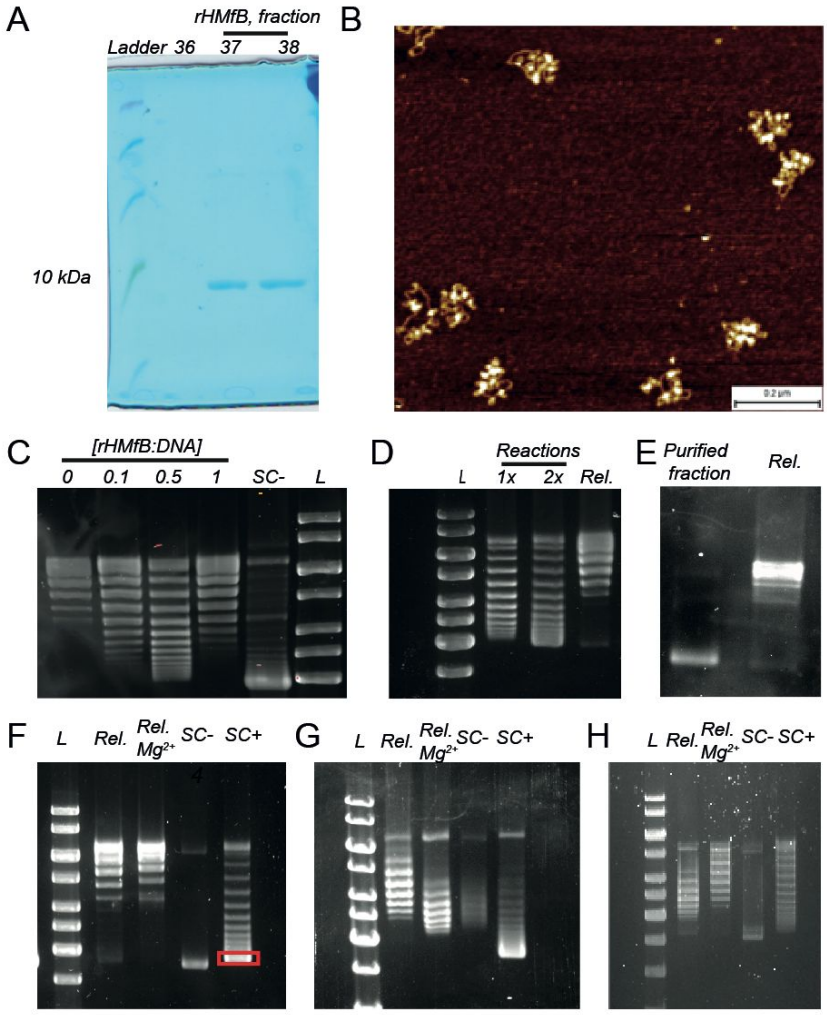

Supporting Figure S2. Generation and characterization of positively supercoiled pBR322. **A.** SDS PAGE of purified rHMfB showing the purity of two different fractions of purified rHMfB. **B.** AFM topograph of rHMfB incubated with relaxed pBR322. **C.** Gel electrophoresis data of pBR322 relaxed in the presence of different concentrations of rHMfB, and negatively supercoiled pBR322 (SC-) and ladder (L). **D.** Gel electrophoresis data of the effect of a single versus dual round of topoisomerization in the presence of rHMfB, as well as the in the absence of rHMfB ("Rel."). **E.** Gel electrophoresis photograph of gel-purified highly positively supercoiled pBR322, and relaxed pBR322. **F.** Comparison of pBR322 relaxed with topoisomerase Ib in assay buffer (50 mM Tris.HCl (pH 7.9), 1 mM EDTA, 1 mM DTT, 20 % (v/v) glycerol, 50 mM NaCl or in AFM deposition buffer ("Rel. Mg^{2+}"), negatively supercoiled pBR322, and positively supercoiled pBR322. The red box indicates the position of the gel excised for purification and AFM analysis. Note that a different gel was used for this purpose. **G.** Gel electrophoresis photograph of pBR322 plasmids in 1xTAE buffer supplemented with chloroquine. Lanes contain samples identical to those in (F). **H.** Gel electrophoresis photograph of pBR322 plasmids in 1xTAE buffer supplemented with $CaCl_2$ (5 mM). Lanes contain samples identical to those in (F).

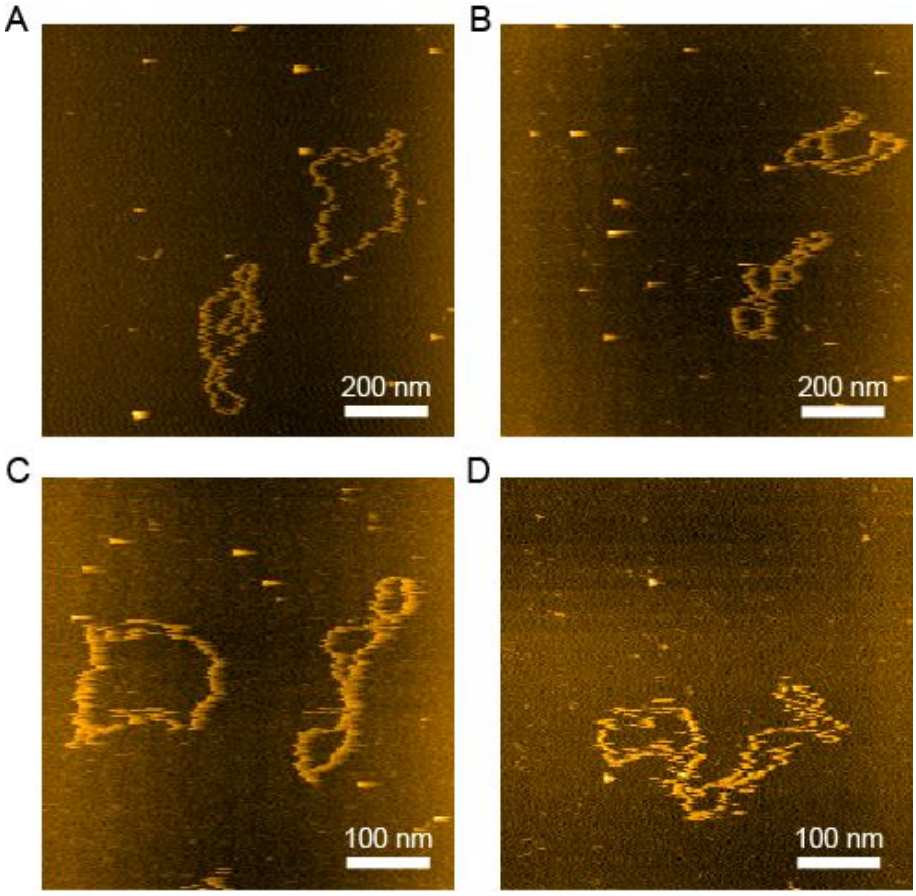

Supporting Figure S3. *In situ* AFM topographs of negatively supercoiled pBR322 deposited on bare mica and imaged in aqueous buffer comprising 5 mM $MgCl_2$.